UNIVERSITY OF COLORADO AT BOULDER

HONOR THESIS

Measurement of PWFA plasma source density using Stark broadening

---

Author:
Shao Xian LEE

Supervisor:
Dr. Mike LITOS

A thesis submitted in fulfillment of the requirements
for the degree of Bachelor of Arts

in the

Department of Physics

April 11, 2019

Declaration of Authorship

I, Shao Xian LEE, declare that this thesis titled, “Measurement of PWFA plasma source density using Stark broadening” and the work presented in it are my own. I confirm that:

- This work was done wholly or mainly while in candidature for a research degree at this University.
- Where any part of this thesis has previously been submitted for a degree or any other qualification at this University or any other institution, this has been clearly stated.
- Where I have consulted the published work of others, this is always clearly attributed.
- Where I have quoted from the work of others, the source is always given. With the exception of such quotations, this thesis is entirely my own work.
- I have acknowledged all main sources of help.
- Where the thesis is based on work done by myself jointly with others, I have made clear exactly what was done by others and what I have contributed myself.

Signed:

Date:

UNIVERSITY OF COLORADO AT BOULDER

Abstract

Department of Physics

Bachelor of Arts

Measurement of PWFA plasma source density using Stark broadening

by Shao Xian LEE

The Plasma Wakefield Accelerator (PWFA) is a type of advanced particle accelerator that can generate high energy particle beams with a reduced footprint and cost compared to conventional accelerators. Recent experiments have shown that the PWFA is able to accelerate an electron beam by 9 GeV in just over a meter. However, to continue making progress the PWFA must be shown to also preserve the beam quality, as quantified by the beam emittance. This requires a carefully tailored plasma source, and therefore, a sufficiently reliable plasma density diagnostic. Stark broadening has been frequently used as a laboratory plasma diagnostic as it provides a fast and reliable approach to determine plasma density and temperature. As the recombined atoms in a plasma de-excite, they release photons and spectral lines are observed. However, when the de-excitation is perturbed by the local electric field of the plasma, the spectral lines are broadened. The full width at half maximum (FWHM) of the broadened spectral line is proportional to the strength of local electric field produced by nearby ions and electrons. The field strength, in turn, is proportional to local plasma density. Therefore, by measuring the FWHM of broadened spectral lines, we are able to indirectly measure the plasma density.

Acknowledgements

I would like to express my heartfelt gratitude to my supervisor Dr. Mike Litos, without whom this project would not have been possible. I would like to also thank my family, especially my mother for supporting me from start to finish.

Contents

List of Figures

To the memory of my father

Chapter 1

Introduction/Background

1.1 Particle Accelerators

Particle accelerators were first developed in the early 20th century for nuclear and particle physics research. As high energy physics theories continue to progress, accelerators that can produce particles at ever higher energies are needed to probe the properties of particles at a smaller and smaller scales. The maximum energy of particle accelerators had been following an exponential trend until the past two decades. As shown in Figure 1.1, recent particle accelerators no longer follow the exponential trend due to the inherent limitations of current accelerator technology.

To build a particle accelerator that is more powerful than the LHC, one needs a space that is larger than a circle with 27km circumference and/or magnets with a field larger than the current limit of 7.7T. Moreover, relativistic charged particles with small mass like the electron suffer high energy loss from synchrotron radiation in the presence of magnetic fields. To prevent energy loss from synchrotron radiation, charged particles with small mass need to be accelerated through a linear accelerator, which does not require strong dipole magnets for turning the beam. However, a linear accelerator that is longer than 50km is needed if we want to accelerate an electron to the high energies of interest to the particle physics community (>1TeV). The accelerating gradient for conventional metallic RF waveguide accelerators is limited by the breakdown induced by the strong electric field produced in the accelerator.

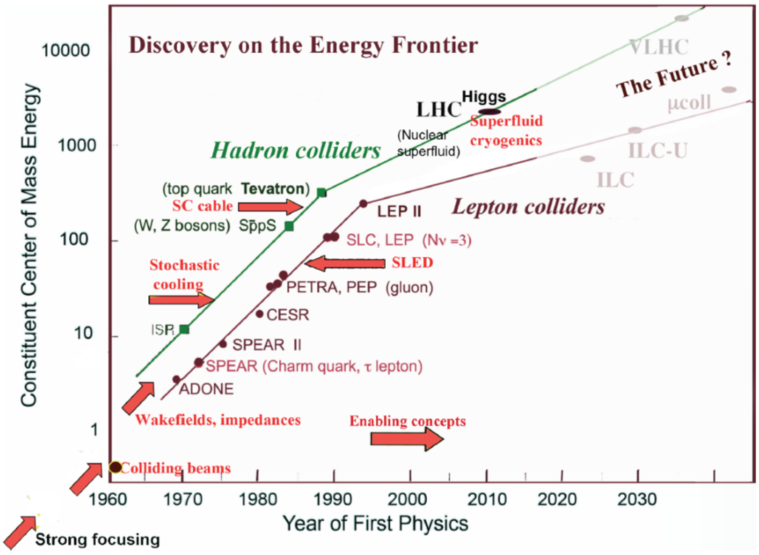

FIGURE 1.1: Livingston plot.[1]

1.2 Plasma Wakefield Acceleration

Plasma Wakefield Acceleration (PWFA) is a next-generation accelerator technique that allows high energy physicists to accelerate particles up to high energy with an accelerator that is 100 to 1000 times smaller than a conventional metallic accelerator without having the concern of breakdown. The concept of accelerating particles using waves in a plasma was first conceived by Toshiki Tajima and John Dawson in 1979 [2] . When a relativistic electron beam is sent into a plasma, the radial Coulomb force produced by the electron beam expels all the nearby plasma electrons as it passes through the plasma. As the ions are much more massive than the plasma electrons, they remain almost stationary when the relativistic electron beam penetrates through the plasma. The plasma electrons are attracted back toward the central axis of the ion column and they set up a periodic wake after the driving electron bunch has passed. For small density perturbations, the frequency of the periodic wake corresponds to the plasma frequency. For large density perturbations in the so-called "blowout regime", as described above, the frequency of the wake is still roughly equal to the plasma frequency.

When a slab of plasma electrons is displaced by some distance, the coulomb

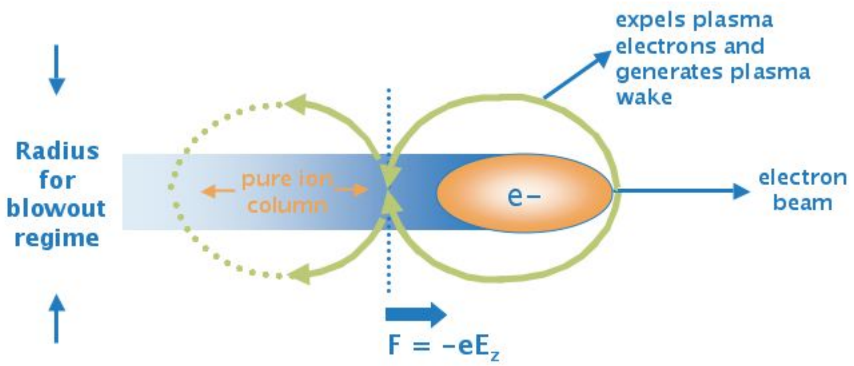

FIGURE 1.2: Diagram of plasma wakefield acceleration.[3]

force produced by the plasma ions pulls back the plasma electrons and they start to oscillate. The frequency of the oscillation is called the plasma frequency:

$$\omega = \sqrt{\frac{n_p^2 e^2}{m\epsilon_0}} \tag{1.1}$$

where n_p is the unperturbed plasma density, e is the charge of electron, m is the mass of electron and ϵ_0 is the permittivity of free space.

The dynamics of the nonlinear blowout plasma can be desribed by Maxwell's equations(cgs) in Lorentz gauge and plasma fluid equations[4][5]:

$$(\frac{1}{c^2}\frac{\partial^2}{\partial t^2} - \nabla^2)\phi = 4\pi\rho \tag{1.2}$$

$$(\frac{1}{c^2}\frac{\partial^2}{\partial t^2} - \nabla^2)\vec{A} = \frac{4\pi}{c}\vec{J} \tag{1.3}$$

$$\frac{1}{c}\frac{\partial\phi}{\partial t} + \vec{\nabla}\cdot\vec{A} = 0 \tag{1.4}$$

$$(\frac{\partial}{\partial t} + \vec{V_i}\cdot\vec{\nabla})\vec{P_i} = q_i(\vec{E} + \frac{V_i}{c}\times\vec{B}) \tag{1.5}$$

where $\rho = \Sigma_i q_i n_i$, $\vec{J} = \Sigma_i q_i n_i V_i$, q_i is the particle charge, V_i is the fluid velocity, and i refers to particle species (ion or electron). ρ and $\vec{J}$ satisfy the charge conservation equation

$$\frac{\partial\rho}{\partial t} + \vec{\nabla}\cdot\vec{J} = 0 \tag{1.6}$$

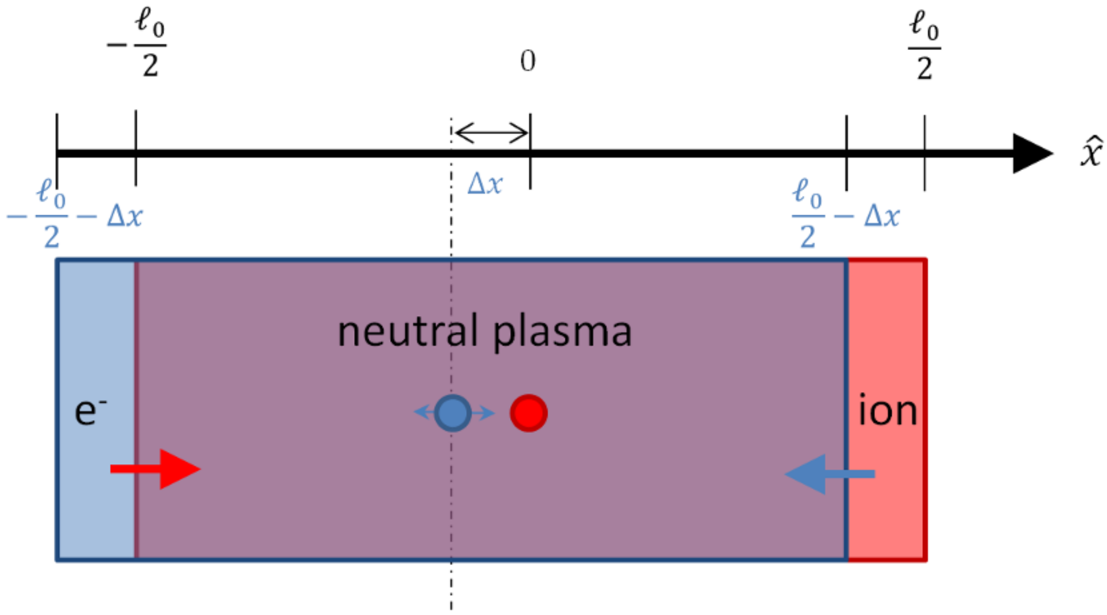

FIGURE 1.3: A slab of plasma electron being displaced by Δx. The slab of electron experiences a pullback force from plasma ions.[6]

These equations can be rewritten under a quasi-static approximation by introducing a new parameter, $\xi = ct - z$. The quasi-static approximation is valid as long as the driver electron beam is relativistic ($\gamma >> 1$), which is the usual case for PWFA. The quasi-static equations are

$$\nabla_\perp^2 \phi = -4\pi\rho \tag{1.7}$$

$$\nabla_\perp^2 A_\perp = -\frac{4\pi \vec{J}_\perp}{c} \tag{1.8}$$

$$\frac{dP_{e\perp}}{d\xi} = \frac{q_e}{1 - V_{e\|}}(E_\perp + (V_e \times B)_\perp) \tag{1.9}$$

Using these equations, we can obtain a trajectory plot like that of figure 1.4. From the plasma electron trajectories, the longitudinal electric field $E(\xi)$ can be calculated. The maximum accelerating field is estimated as[7]

$$E_{max} \simeq 0.96\,\mathrm{GeV/m}\sqrt{\frac{n_p}{10^{18}\,\mathrm{cm}^{-3}}} \tag{1.10}$$

Equation 1.10 tells us that if we place an electron bunch in a blowout wake in a plasma with density $n_p = 10^{16} cm^3$, the electrons can gain an energy of

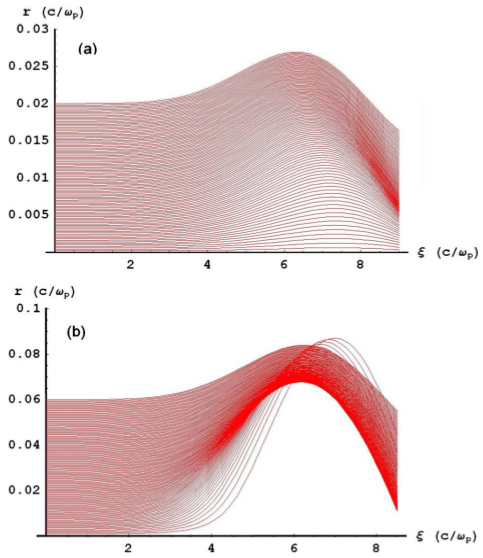

FIGURE 1.4: Plots of trajectories with charge density $n_b = 1$ and $n_b = 10$ from Lu[4]

roughly 10 GeV in 1 m of distance.

1.3 Plasma Source

Discharge ionization by DC voltage is a common way to create a pre-ionized plasma source in the lab. However, this method only works well for low density gas. For example, the voltage required to discharge ionize helium increases rapidly after 0.5 kPa-cm as shown in figure 1.5. For higher density gas used in PWFA, it often requires a very high voltage to discharge the gas. In addition, problems like instability and excessive heat appear when we try to use high voltage breakdown. Compared to discharge ionized-plasma, ionizing a gas using a high power laser pulse provides more control over the plasma characteristics. Therefore, future PWFA experiments will attempt to use a laser-ionized plasma source. A 10TW, 800nm wavelength Ti:Sapphire laser is used for laser-ionized plasma source research and development in our lab. Our ideal plasma source is a filament, 1m long and 1mm in diameter. The target plasma density and temperature of the plasma source are $10^{16} cm^3$ and 1eV, respectively.

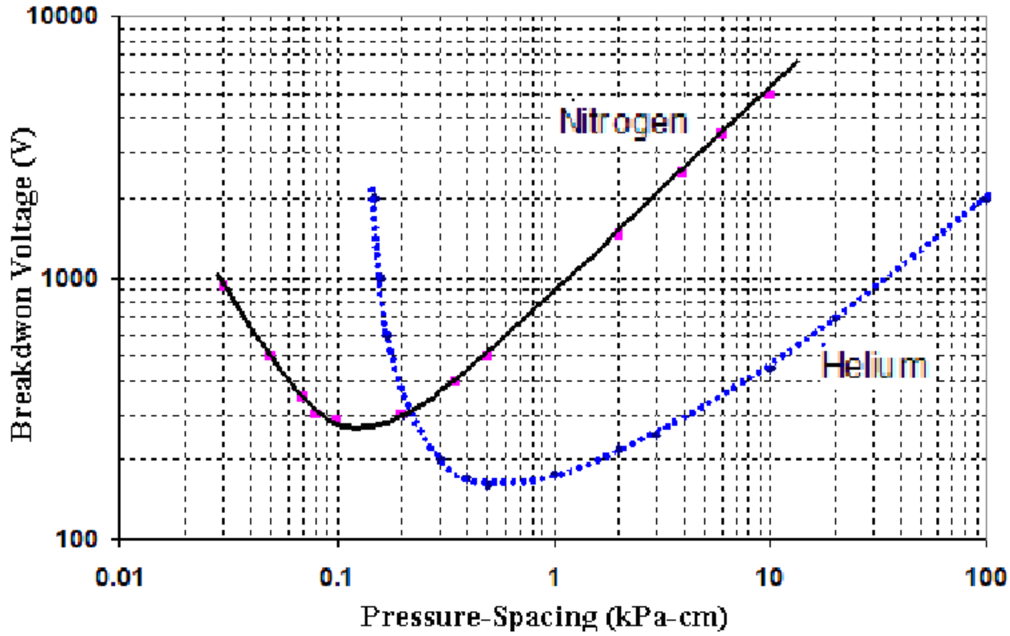

FIGURE 1.5: Paschen Curves for nitrogen and helium. The breakdown voltages are the lowest for nitrogen and helium at 0.1 kPa-cm and 0.5 kPa-cm,respectively.[8]

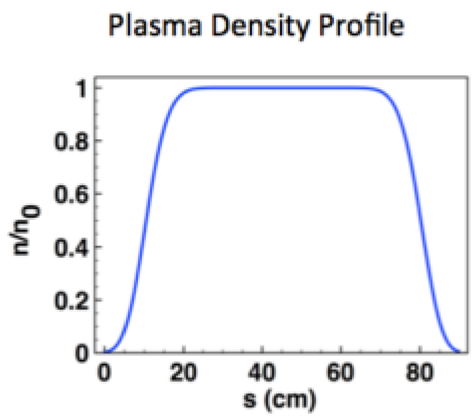

FIGURE 1.6: Laser ionized-plasma density profile of a PWFA experiment carried in SLAC.[9]

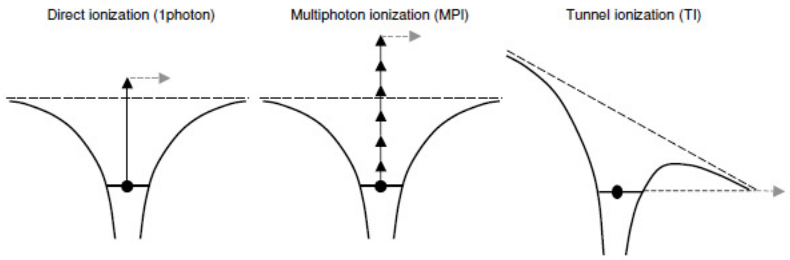

FIGURE 1.7: A comparison between direct ionization, multiphoton ionization and tunnelling ionization. The potential barrier for tunnelling ionization is lower compared to other two methods.[10]

1.4 Tunnelling ionization

The laser in our lab utilizes tunnelling ionization to ionize the gas. Tunnelling ionization is a quantum mechanical process in which the electrons in an atom escape the nuclear Coulomb potential, despite having an energy below the potential energy barrier. If an electric field is present, the potential barrier of an atom is distorted and can dip below the electron energy at some distance from the atom as shown in Figure 1.7. This makes it possible for an electrons in the atom to tunnel through the barrier via quantum tunnelling. Tunnelling ionization is different from multi-photon ionization because it does not require the electrons in the atom to obtain energy above the threshold ionization energy, and is therefore a more effective means of ionization with an infrared laser.

1.5 Plasma diagnostic

Equation 1.10 tells us that the maximum accelerating field is proportional to the plasma density. In other words, if we want to know how much we can accelerate an electron beam, we must know what the plasma density is. This motivates us to diagnose the plasma density before the arrival of the driver electron beam. Methods like interferometry and spectral line broadening are developed to measure plasma density. In this thesis, I will use Stark broadening to measure the density of the PWFA plasma source.

Chapter 2

Stark Broadening

2.1 Stark broadening

As the electrons in recombined atoms de-excite, they release photons and spectral lines are observed. If the de-excitation is perturbed by local fields, the spectral lines are broadened as shown in figure 2.1.

One of the commonly observed spectral line broadenings in plasma is Stark broadening. Stark broadening has been frequently used by plasma physicists as it provides a fast and reliable approach to determine plasma density and temperature. Stark broadening or the Stark effect is the broadening of spectral lines due to the local electric field produced by the nearby ions and electrons. The average strength of the local electric field is determined by the plasma density. Thus, we are able to infer the plasma density from the measured broadening of spectral lines. The Stark effect for hydrogen and hydrogenic atoms is linear, i.e. the full width half maximum (FWHM) is directly proportional to the field distribution. Meanwhile, the Stark effect for other elements is quadratic. The Stark broadening model can be divided into two parts: the quasi-static approximation and impact broadening theory.

2.2 Quasi-static approximation

Under the assumption that the plasma is in equilibrium, the ions are moving much slower than the electrons, as they have larger mass. The ions are considered ‘static’ relative to the timescale of the lifetime of atomic excited

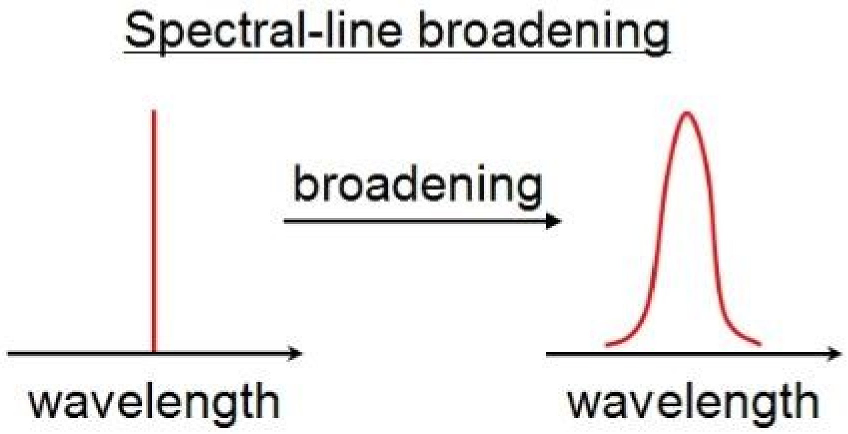

FIGURE 2.1: The broadening of spectral line[11]

states. As a result, the changes of microfield are slow and we can assume the low frequency electric field is time-independent. The spectral line profile can be estimated by the quasi-static approximation [12][13]. The calculation for electric field produced by ions is rather complex. Holtsmark simplified the calculation by stating two assumptions:

1. Perturbers (ions) are uncorrelated with themselves and with the emitter.
2. The emitter only experiences the field from the closest perturber.

The calculated normal field strength using Holtsmark field model is:

$$F_0[\frac{V}{m}] = 3.748 \times 10^{-9} Z_p N^{\frac{2}{3}} \tag{2.1}$$

and the Holtsmark field distribution is:

$$H(\beta) = \frac{2}{\pi} \int_0^{\infty} x sin(\beta x) exp(-x^{\frac{3}{2}}) dx \tag{2.2}$$

where Z_p is the nuclear charge, $\frac{E}{F_0}$ (normalized field), E is the coulomb field produced by the perturber and N is the number density of plasma. Figure 2.2 shows the Holtsmark field distribution, which represents a probability distribution function for an emitter to experience a particular field strength. It can be seen from Figure 2.2 the distribution is sharply peaked at 1.6 β, thus

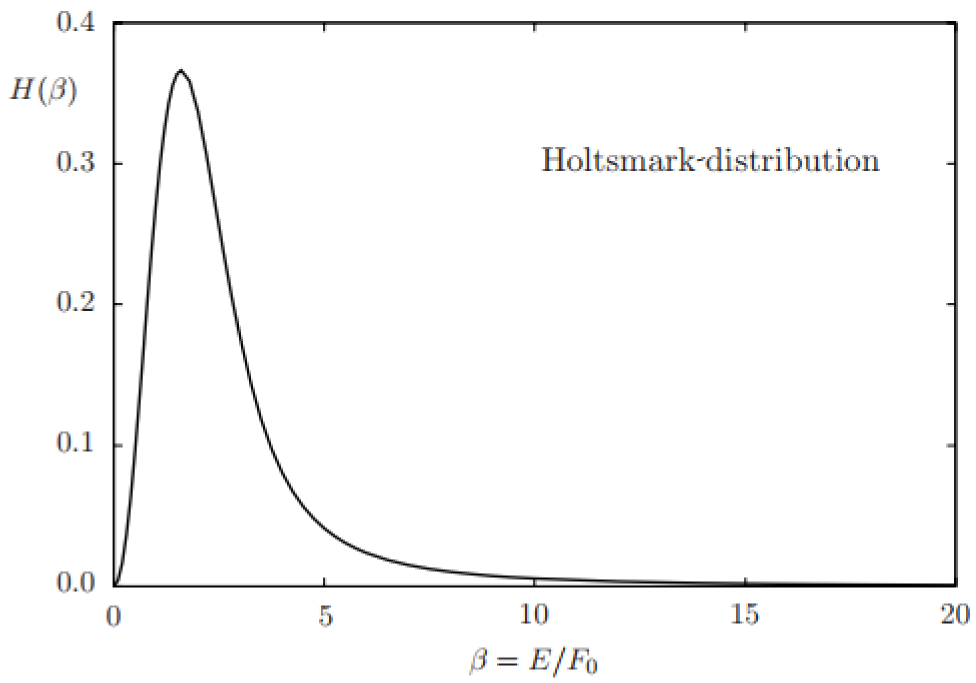

FIGURE 2.2: The Holtsmark distribution[11]

it is reasonable to approximate all emitters as having the field strength of roughly 1.6 F_0. Under this assumption, we can say the FWHM of the spectral line is proportional to $N^{\frac{2}{3}}$. In reality, we have to integrate over the whole distribution and the FWHM may not be exactly proportional to $N^{\frac{2}{3}}$.

2.3 Impact broadening theory

As the electrons are moving faster than the ions, the quasi-static approximation does not work for the high frequency electric field produced by the electrons. The broadening of spectral lines caused by Coulomb collisions of electrons can be approximated by impact broadening theory. Impact broadening theory requires the collisional time to be shorter than the atomic deexcitation time. As mentioned by Fujimoto[3], the Lorentzian electron impact broadening profile is:

$$I(\omega) = \frac{\gamma}{2\pi} \frac{1}{(\omega - \omega_0 - \Delta)^2 + (\frac{\gamma}{2})^2} \tag{2.3}$$

where ω_0 is the central frequency, $\Delta = n_e < \sigma v_e >$ (displacement of the line), $\frac{\gamma}{2} = n_e < \sigma v_e >$, $< v_e >$ is the average speed of the electrons, n_e is the electron density, is the cross section for electron collision, and v_e is the thermal velocity of the plasma electrons.

2.4 Comparison between quasi-static broadening and impact broadening

To compare quasi-static broadening and impact broadening, we can introduce the parameter

$$h = \Delta\omega\tau \sim \frac{\Delta\omega}{\gamma} \tag{2.4}$$

where $\gamma \sim \frac{1}{\tau}$ is the impact broadening width, and τ is the mean free time between successive collision. The quasi-static frequency shift, $\Delta\omega$ in the linear Stark effect is proportional to the electric field strength, and in the quadratic Stark effect it is proportional to the square of the field strength. Furthermore, the impact broadening frequency shift, ω is proportional to the Weisskopf radius. The Weisskopf radius, $r_w = \frac{\hbar n_h^2}{mv}$, determines the strength of the collisions, where n_h is the upper principal quantum number. It corresponds to the impact parameter where the collision of the particle becomes weak. Combining all the relationships, we can rewrite equation 2.4 as

$$h^3 = \left(\frac{r_w^3}{r_m^3}\right)^{n_s-1} \sim \left(\left(\frac{\hbar n_h^2}{m_e}\sqrt{\frac{m}{2kT}}\right)^3 N\right)^{n_s-1} \tag{2.5}$$

where r_m is the average distance to the closest perturber, and $n_s = 2$ for linear effect and $n_s = 4$ for quadratic Stark effect. Equation 2.5 shows that if $h^3 << 1$, impact broadening is dominant. Meanwhile, if $h^3 >> 1$, the quasi-static approximation is dominant. For example, if we plug in n=4 (Balmer β line), T=10000K and $N = 10^{22}m^{-3}$ for hydrogen ion, we get $h^3 \sim 30$. Therefore, the quasi-static contribution to line broadening dominates for this case.

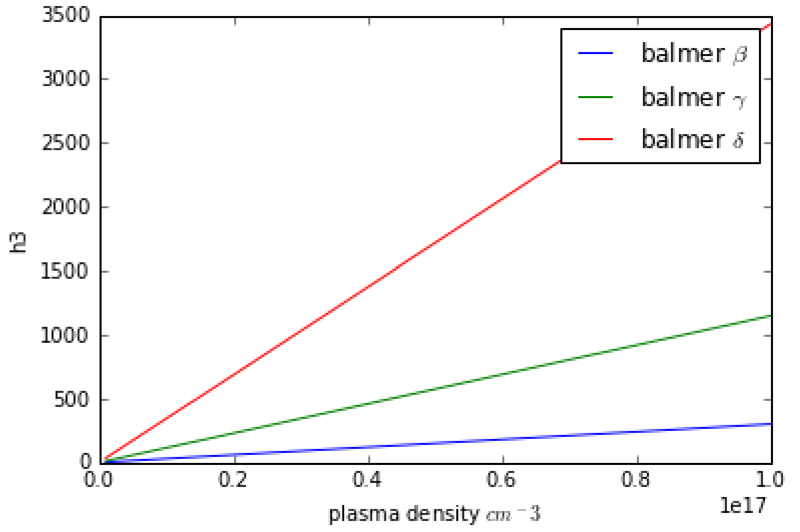

FIGURE 2.3: h^3 for Balmer β,γ,δ lines at T=10000K at different plasma density

2.5 Hydrogen spectral lines

The Stark broadening model consists of the quasi-static approximation and impact broadening theory. However, as shown in figure 2.3, h^3 is much greater than 1 for the hydrogen Balmer β, γ, and δ lines at T=10000K and $N = 10^{22}m^{-3}$. The quasi-static approximation is dominant for hydrogen ions and the electron impact broadening effect can be neglected for this case. The full width half maximum for the hydrogen spectral profile is therefore

$$\Delta\omega_{1/2}[Hz] \approx 13.7\frac{\hbar}{m_e}\frac{z}{Z}(n_p^2 - n_q^2)n_z^{\frac{2}{3}} \tag{2.6}$$

or in units of wavelength

$$\Delta\lambda_{1/2}[nm] \approx 8.4 \times 10^{-22}\lambda_{pq}^2\frac{z}{Z}(n_p^2 - n_q^2)n_z^{\frac{2}{3}} \tag{2.7}$$

where m_e is the mass of the electron, Z is the nuclear charge of the emitting ion, z is the charge of the perturber ion, n_z is the plasma density, n_p is the principal number of the higher state, n_q is the principal number of the lower state and λ_{pq} is the central wavelength. The parameter $\alpha_{1/2} = 8.4 \times$

$10^{-22}\lambda_{pq}^2 \frac{z}{Z}(n_p^2 - n_q^2)$ is obtained from the actual calculation for the quasi-static approximation using the Holtsmark distribution. $\alpha_{1/2}$ is independent of temperature because the Holtsmark distribution considers the ions to be static. In reality, the FWHM is slightly dependent on temperature and is usually smaller than the above approximation because the Holtsmark distribution ignores ion-ion interactions and Debye screening. For non-hydrogenic atoms, the electron impact broadening can play an important role and cannot always be neglected. In general, the quasi-static approximation contributes only to the wings of spectral line at $\omega - \omega_0 > \lambda$ and impact broadening contributes to the central portion of spectral line $\omega - \omega_0 \leq \lambda$. If the contribution from impact broadening is small, λ will be very narrow and we can ignore its contribution.

2.6 Inglis-Teller relation

Using equation 2.5, we can show that the coulomb collisional effect from electrons is not dominant at low plasma temperature. Instead, the broadening effect by electrons comes from the quasi-static Stark effect. In this case, the perturbers are both ions and free electrons. The maximum separation of adjacent atomic energy levels from the Stark effect is

$$\Delta E = 3F_0 e a_0 \frac{n(n-1)}{Z} \tag{2.8}$$

where n is the principal quantum number, e is the elementary charge and a_0 is the Bohr radius. In the presence of a strong enough field, the Balmer lines will merge and form a continuous spectrum due to the Stark effect. This phenomenon occurs when the maximum separation of atomic energy level from Stark broadening is equal to one-half the energy difference of levels n to n+1. We equate equation 2.8 to the Rydberg equation for a transition between

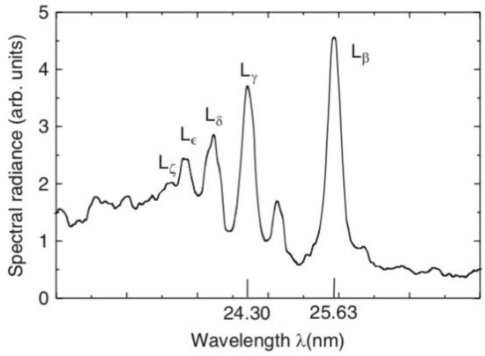

FIGURE 2.4: He II spectrum from hydrogen plasma

levels n and n+1

$$3F_0ea_0\frac{n(n-1)}{Z} = \frac{e^2}{2a_0}Z^2\left(\frac{1}{n^2} - \frac{1}{(n+1)^2}\right) \tag{2.9}$$

By substituting equation 2.1 to 2.9, we obtain[15]

$$\log N = 23.491 - 1.5\log|Z_p| + 4.5\log Z - 7.5\log n_m \tag{2.10}$$

where n_m is the maximum principal quantum number. Using this equation, we can easily estimate the plasma density from the highest energy of observable transition lines. For example, as shown in figure 2.4, the last resolvable line from the Lyman series of He-II emitted from a He-doped (Z=2) hydrogen plasma is L ($n_m = 6$). The estimated density is therefore $4.4 \times 10^{18} cm^{-3}$. The Inglis-Teller relation provides us a tool to quickly estimate the plasma density.

2.7 Doppler effect

As the recombined atoms in the plasma move around, the Doppler effect also broadens the spectral lines, producing a Gaussian line broadening. The full width half maximum for the Doppler broadening profile is

$$\Delta\lambda[nm] = 7.16 \times 10^{-7}\lambda_0\sqrt{\frac{T}{M}} \tag{2.11}$$

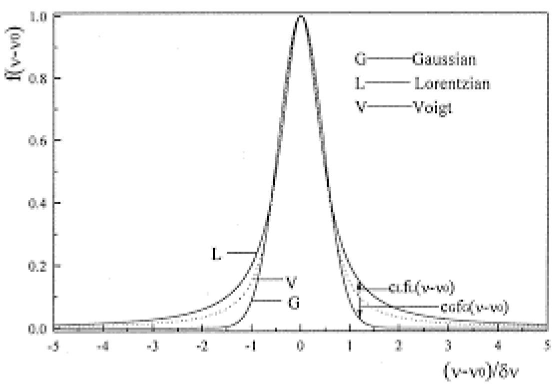

FIGURE 2.5: The Gaussian function, Lorentzian function and Voigt function

where T is plasma temperature in K, and M is the mass of the atom in atomic mass units. The spectral line profile, which includes Stark and Doppler effects, should be modelled using a Voigt function, which is a convolution of a Gaussian function (Doppler) and a Lorentzian function (Stark) as shown below

$$V(x;\sigma,\gamma) = \int_{-\infty}^{\infty} G(x';\sigma)L(x-x' : \gamma)dx' \tag{2.12}$$

where G is the Gaussian function, and L is the Lorentzian function. Figure 2.5 shows the comparison between a Gaussian function, a Lorentzian function and a Voight function. At low plasma temperature (e.g. T=10000K), the Doppler broadening width is negligible.

Chapter 3

Experimental setup and results

3.1 Experimental setup

This basic experimental setup is presented in figure 3.1 . There are two gas-filled vacuum chambers used in this experiment. Chamber 1 contains the optics for the laser system, and Chamber 2 contains the laser-ionized plasma. The gas pressure can be controlled, and is read out by a cold cathode gauge with 30% accuracy. A 1m long plasma filament with 1mm diameter can be created in Chamber 2 using an 800nm, 10 TW peak-power Ti:Sapphire laser and axicon lens. The laser is pulsed at 10 Hz, and has a pulse length of approximately 30 fs. The axicon lens is used to create the plasma filament because it allows us to turn a flat-top laser beam into a Bessel-like beam as shown in figure 3.2. The Bessel-like focus can be sustained over a long distance which permits the creation of a long plasma filament. If the laser fully ionizes the gas along its focal region, the density will be uniform and its value will be determined by the neutral gas pressure in the chamber.

To observe the spectrum of the plasma, a Tokina AT-X 100mm macro lens is used to focus the emission light into an optical fiber connected to an Ocean Optics HR4000 spectrometer (wavelength range:220-1100nm, resolution:0.1nm).

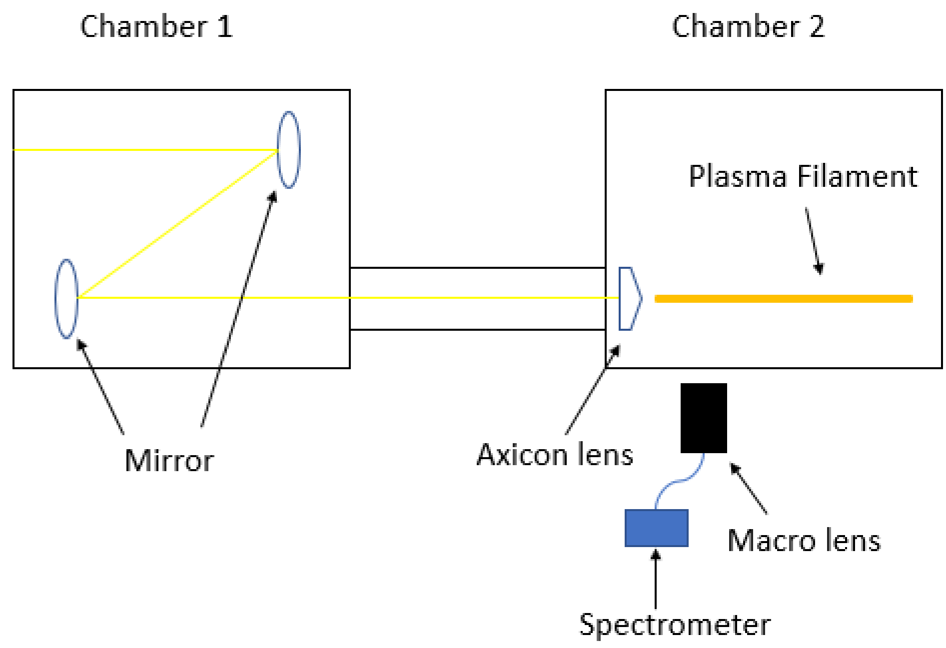

FIGURE 3.1: Overview of experimental setup.

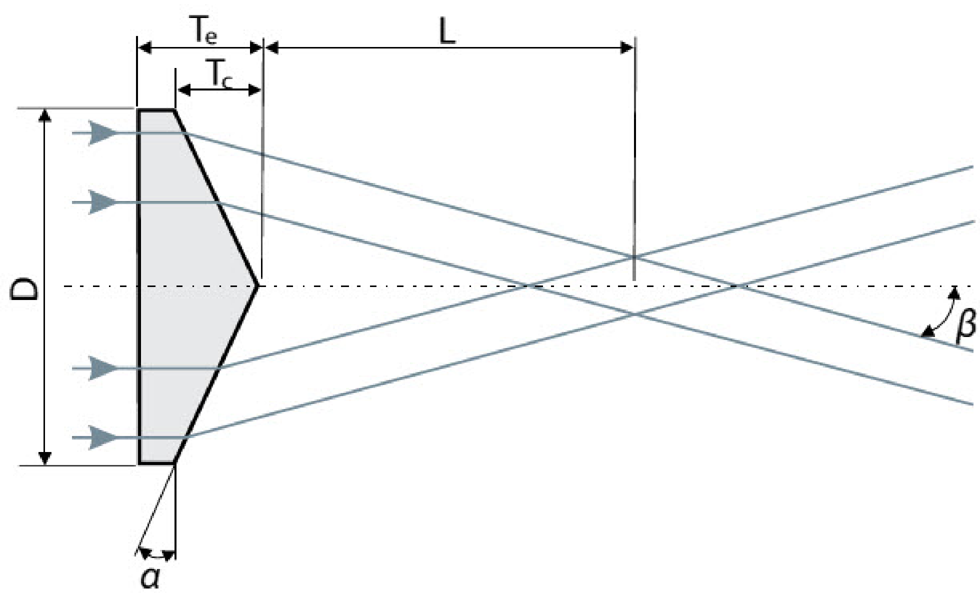

FIGURE 3.2: Axicon focus of a laser beam.[16]

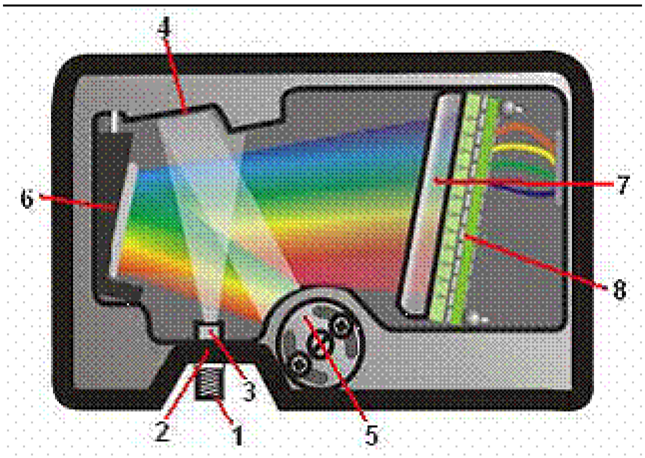

FIGURE 3.3: Interior look of spectrometer.Number 3, 6, 8 represent the slit, diffraction grating and CCD camera, respectively.[17]

3.2 Spectrometer

A spectrometer has three main components: a slit, a diffraction grating, and a CCD chip. In our setup, as is often the case, the light is coupled into the spectrometer with an optical fiber. The light enters through the slit and strikes the diffraction grating. The diffraction grating then disperses the photons by wavelength, sending them on to the CCD camera. Figure 3.3 shows a diagram of a spectrometer similar to the one used in this experiment. The resolution of the spectrometer is determined by the width of the slit, the line density of the grating, and the pixel density of the CCD. For example, the smaller the slit size, the better the resolution. Similarly, the higher the grating line density, the better the resolution.

3.3 Experimental result

In the experiment, we ionized helium gas to create the plasma source. We assume the helium gas is fully ionized based on calculations using the ADK approximation, taking the laser intensity and pulse length into account. It is challenging to achieve a good signal-to-noise ratio with a single shot due to the geometry of the setup and the signal attenuation in the fiber and spectrometer. The plasma emission light is isotropic, and the lens subtends an

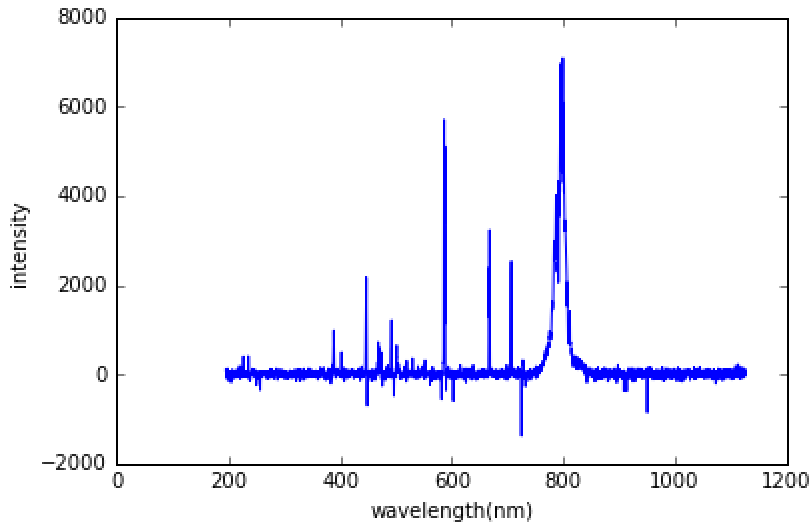

FIGURE 3.4: Helium plasma spectrum with laser spectral line at 800nm.

TABLE 3.1: calculated line widths for various initial densities.

Gas density(cm^{-3})	**Measured FWHM(nm)**	**Calculated plasma density(cm^{-3})**
4.86×10^{16}	0.208	$4.95{\times}10^{16}$
6.56×10^{16}	0.250	$6.18{\times}10^{16}$

angle of $24°30'$, which gives a geometric collection efficiency of about 3%. To enhance the signal, the spectrum of plasma is integrated over 1000 shots (100 seconds). The observed spectrum of helium plasma obtained for gas density $n_0 = 4.86 \times 10^{16} cm^{-3}$ is shown in Figure 3.4. In this experiment, we focus on the He Paschen α line, P_α, at 468.56nm. The relation between the FWHM and plasma density for this line is[18]

$$\Delta\lambda_{\frac{1}{2}}[nm] \simeq 2.74 \times 10^{-20}(n_p)^{0.831} \tag{3.1}$$

A Lorentzian function is fit to the P_α line for gas density $4.86 \times 10^{16} cm^{-3}$ and $6.56 \times 10^{16} cm^{-3}$ as shown in figure 3.5 and 3.6. A comparison of the calculated plasma density to the measured gas density is shown in Table 3.1. As can be seen, the measured plasma densities are well within the 30% uncertainty of the pressure gauge reading.

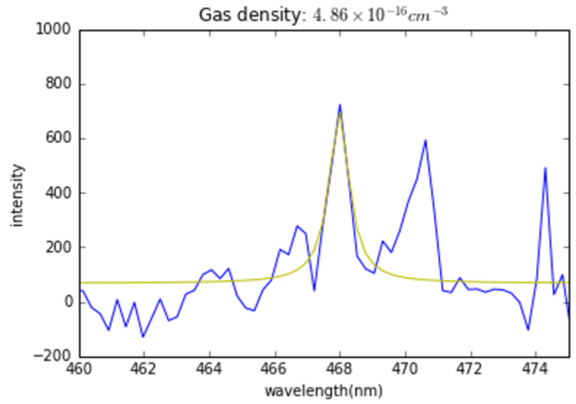

FIGURE 3.5: He P_α at $n_0 = 4.86 \times 10^{16} cm^{-3}$

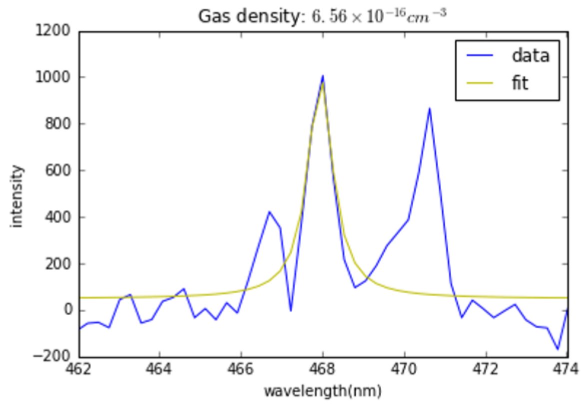

FIGURE 3.6: He P_α at $n_0 = 6.56 \times 10^{16} cm^{-3}$

Chapter 4

Conclusions & Future Plans

4.1 Conclusions

A controlled test of the Stark broadening diagnostic was performed where a plasma with a known density was formed and measured. The plasma density for two different neutral gas densities, $4.86 \times 10^{16} cm^{-3}$ and 6.56×10^{16}, were calculated by measuring the FWHM of the He P_α line. The diagnostic provided density readings within the 30% uncertainty of the pressure gauge reading that was used to measure the controlled neutral gas density. Based on these results, the diagnostic should be able to provide accurate measurements of the PWFA plasma source, even where the gas is only partially ionized.

4.2 Future plans

Several steps can be taken to improve the accuracy of the plasma density measurement in the future:

1. The resolution of spectrometer can be improved by reducing the slit width and increasing the grating density. The best resolution expected from commercially available spectrometers for the Paschen Alpha line is 0.06 nm.

2. Can improve the optical collection efficiency with a different lens and the use of mirrors. This will reduce the number of shots required for good signal-to-noise ratio.

3. Can reduce the minimum single shot time integration window from $\sim 100\mu s$ to a few nanoseconds if an ICCD is implemented. This reduces the degree of change in the plasma density during the integration window due to recombination. With a fast shutter ICCD, the temporal evolution of the plasma need not be taken into account.

4. If an expensive ICCD spectrometer is not available, a model of the plasma decay can be used to take the time evolution of the density into account. This technique is described in further detail in the following section.

4.2.1 Time-resolved Stark broadening profile

When a high intensity laser pulse propagates through gas, the laser pulse ionizes the gas via tunnelling ionization and a plasma is created. Shortly after the plasma is created, the plasma starts to recombine. Because the plasma recombines faster than the shutter speed of the spectrometer, it is impossible to measure a signal from only the fully ionized plasma. To resolve this problem, a time dependent plasma recombination model is constructed. In this model, the relationship between gas density (or recombined plasma density), n_r and plasma density, n_p can be described using two ordinary differential equations[19]:

$$\frac{dn_p}{dt} = -\alpha n_p^2 \tag{4.1}$$

$$\frac{dn_r}{dt} = \alpha n_p^2 \tag{4.2}$$

where α is the temperature dependent recombination coefficient. This model allows us to calculate the time integrated spectral profile over the entire duration of the spectrometer observation time.

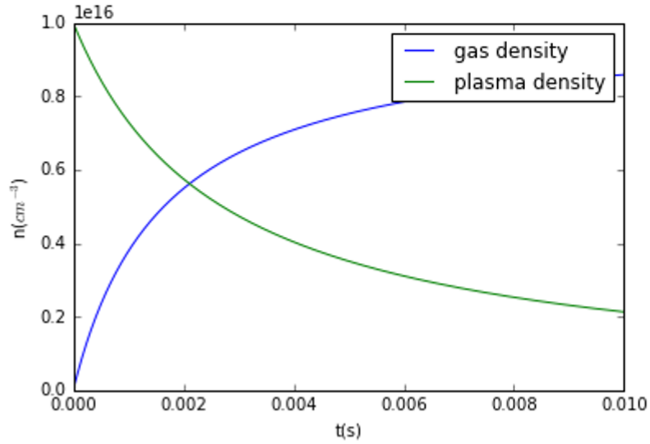

FIGURE 4.1: Gas density, plasma density versus time plot for initial plasma density,$n_0 = 10^{22} cm^{-3}$

4.2.2 Recombination coefficient

Radiative recombination and three-body recombination are the two most common recombination processes that occur in plasma. Radiative recombination happens when a plasma electron is captured by an ion and releases one photon. Three-body recombination occurs when a second plasma electron carries away the excess energy created by the capture of the first electron by an ion. The reaction equation for this process is

$$e + e + A^+ \rightarrow A + e \tag{4.3}$$

where A^+ is the ion. As our plasma has high density, i.e. $10^{16} cm^{-3}$, it is safe to assume that three-body recombination is dominant until few ions are left. Makin and Keck [20] used classical variational method to calculate the recombination rate of optically thin hydrogen and helium plasmas. They treated the motion of the three bodies as a point in 18-dimensional phase space. In this theory, the interactions between electrons and ions are assumed to be within a range r_0 in which the potential of the electron-ion recombining pair is equal to or larger than the mean thermal energy. The expression for the recombination coefficient obtained from this theory has the form of[21]

$$\alpha = A + BT^{-\frac{9}{2}} n_p \tag{4.4}$$

TABLE 4.1: calculated line widths for various initial densities.

Gas density(cm^{-3})	**Plasma density at 0.1μs(cm^{-3})**	**FWHM at 0.1μs(nm)**
1×10^{14}	9.9996×10^{13}	1.14×10^{-3}
5×10^{14}	4.9988×10^{14}	4.35×10^{-3}
1×10^{15}	$9.9933\times{}^{1}0^{14}$	7.74×10^{-3}
5×10^{15}	$4.9491\times{}^{1}0^{15}$	2.92×10^{-2}
1×10^{16}	$9.6343\times{}^{1}0^{15}$	5.08×10^{-2}
5×10^{16}	$2.6525\times{}^{1}0^{15}$	1.18×10^{-1}

where A and B are constants.

4.2.3 Simulation

Table 4.1 shows the calculated He P_α FWHM using equation 3.1 and the plasma recombination model for different gas densities at $t = 1\mu s$. According to Drawin and Emard[21], the recombination coefficient at T=1eV is

$$\alpha[\frac{cm^3}{s}] = 3.2 \times 10^{-13} + 6.8 \times 10^{-10} T^{-\frac{9}{2}} n_e \tag{4.5}$$

The gas is assumed to be fully singly ionized. The FWHM increases as the gas density increases due to an increase in the strength of the local electric field as predicted by the theory presented in the Stark broadening theory section.

Chapter 5

Bibliography

1. A. Barletta, W Bai, Mengjie Battaglia, M Bruning, O Byrd, John Ent, R Flanagan, John Gai, Weiya Galambos, J Hoffstaetter, G Hogan, M Klute, M Nagaitsev, S Palmer, Mark Prestemon, Soren Roser, Thomas Rossi, L Shiltsev, Vladimir Varner, G Yokoya, K. (2014). Planning the Future of U.S. Particle Physics (Snowmass 2013): Chapter 6: Accelerator Capabilities.

2. TAJIMA, T., DAWSON, J. M. (1979). Laser electron accelerator. Physical Review Letters, 43(4), 267-270. doi:10.1103/PhysRevLett.43.267

3. E164 E164X:PLASMA WAKEFIELD ACCELERATOR EXPERIMENT Retrieved from http://www.slac.stanford.edu/grp/arb/e164/OVERVIEW.htm

4. Lu, W., Huang, C., Zhou, M., Tzoufras, M., Tsung, F., Mori, W., Katsouleas, T. (2006). A nonlinear theory for multidimensional relativistic plasma wave wakefields. Physics of Plasmas, 13(5), 56709. doi:10.1063/1.2203364

5. Huang, C., Lu, W., Zhou, M. M., Decyk, V. K., Mori, W. B., Oz, E., . . . O'Connell, C. (2004). Simulation of a 50GeV PWFA stage. Paper presented at the , 737 433-439. doi:10.1063/1.1842574

6. Schiff, C. (n.d.). Plasma Oscillations. Retrieved from http://underthehood.blogwyrm.com/?p=886

7. Esarey, E., Sprangle, P., Krall, J., Ting, A. (1996). Overview of plasma-based accelerator concepts. IEEE Transactions on Plasma Science, 24(2), 252-288. doi:10.1109/27.509991

8. Sozer, E.B.. (2008). Gaseous Discharges and Their Applications as High Power Plasma Switches.

9. Hogan, M. FACET-II Science Workshop Summary Report (2016) Retrieved from http://slac.stanford.edu/pubs/slacreports/reports21/slac-r-1078.pdf

10. Strong fields http://faculty.chem.queensu.ca/people/faculty/stolow/research/StrongFields.html

11. Atomic Transitions II Molecular Structure Retrieved from https://apatruno.files.wordpress.com/2016/09/lecture121.pdf

12. Griem, H. R. (1974). Spectral line broadening by plasmas. New York: Academic Press.

13. Gigosos, M. (2014). Stark broadening models for plasma diagnostics. Journal of Physics d-Applied Physics, 47(34), 1-33. doi:10.1088/0022-3727/47/34/343001

14. Kunze, H. (2009). Introduction to plasma spectroscopy (1. Aufl. ed.). Heidelberg;New York;: Springer. doi:10.1007/978-3-642-02233-3

15. Mitrofanov, A. V. (1973). On a Revised Version of the Inglis-Teller Formula. Soviet Astronomy, Vol. 16, p.867

16. 14APX-1-90-1 - Plano-Convex Axicon Lenses Retrieved from https://www.findlight.net/optics/lenses/axicons/14apx-1-90-1-plano-convex-axicon-lenses

17. USB2000 Specifications Retrieved from https://chemistry.oregonstate.edu/courses/ch361-464/ch461/ocean%20optics%20spectromete

18. Pittman, T.L., Fleurier, (1986) Plasma shifts of the He II H_α and P_α lines C.Phys Rev A Gen Phys. 1986 Feb;33(2):1291-1296

19. Shirai, H., Tabei, K. (1973). Measurements of the electronic recombination coefficient in a helium plasma jet. Physical Review A, 7(4), 1402-1407. doi:10.1103/PhysRevA.7.1402

20. Makin, B., Keck, J. C. (1963). Variational theory of three-body electron-ion recombination rates. Physical Review Letters, 11(6), 281-283.

21. Drawin, H. W., Emard, F. (1975) Comparative study of existing theories for volume ion-electron recombination in plasmas. Beitraege aus der Plasmaphysik, vol. 15, no. 6, 1975, p. 273-290.